JACS
JOURNAL OF THE AMERICAN CHEMICAL SOCIETY

Article

pubs.acs.org/JACS

Differentiating Left- and Right-Handed Carbon Nanotubes by DNA

Geyou Ao,[†] Jason K. Streit,[†] Jeffrey A. Fagan, and Ming Zheng*

Materials Science and Engineering Division, National Institute of Standards and Technology, 100 Bureau Drive, Gaithersburg, Maryland 20899, United States

Supporting Information

ABSTRACT: New structural characteristics emerge when solid-state crystals are constructed in lower dimensions. This is exemplified by single-wall carbon nanotubes, which exhibit a degree of freedom in handedness and a multitude of helicities that give rise to three distinct types of electronic structures: metals, quasi-metals, and semiconductors. Here we report the use of intrinsically chiral single-stranded DNA to achieve simultaneous handedness and helicity control for all three types of nanotubes. We apply polymer aqueous two-phase systems to select special DNA-wrapped carbon nanotubes, each of which we argue must have an ordered DNA structure that binds to a nanotube of defined handedness and helicity and resembles a well-folded biomacromolecule with innate stereoselectivity. We have screened over 300 short single-stranded DNA sequences with palindrome symmetry, leading to the selection of more than 20 distinct carbon nanotube structures that have defined helicity and handedness and cover the entire chiral angle range and all three electronic types. The mechanism of handedness selection is illustrated by a DNA sequence that adopts two distinct folds on a pair of (6,5) nanotube enantiomers, rendering them large differences in fluorescence intensity and chemical reactivity. This result establishes a first example of functionally distinguishable left- and right-handed carbon nanotubes. Taken together, our work demonstrates highly efficient enantiomer differentiation by DNA and offers a first comprehensive solution to achieve simultaneous handedness and helicity control for all three electronic types of carbon nanotubes.

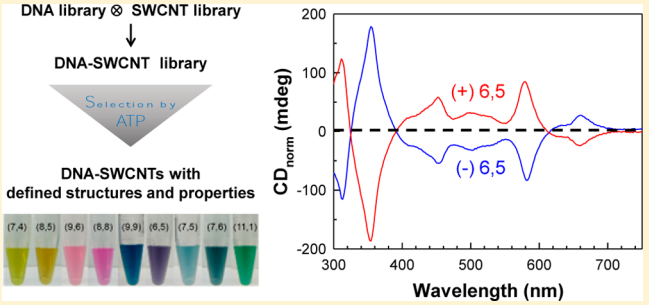

INTRODUCTION

No scalable synthesis solution is currently available for making single-wall carbon nanotubes (SWCNTs) with defined structure and properties despite the progress made in recent years.[1−3] Indeed, synthesis typically produces over 30 distinct species, of which about two-thirds are semiconducting and one-third are quasi-metallic or true metallic, each with different material properties. Postsynthesis sorting methods reported to date have provided a partial solution to the problem.[4−10] In particular, simultaneous helicity and handedness control has been demonstrated, but for only a small number of semiconducting tubes and with a limited degree of enrichment.[11−17] The work to be presented in this paper aims at a comprehensive method for achieving simultaneous helicity and handedness control for all three electronic types of SWCNTs. To avoid confusion in terminology, we define (n, m) and (m, n) tubes as having the same *helicity* but different *handedness*. Our approach makes use of DNA, a sequence-controlled homochiral polymer that can fold onto a SWCNT to form stable: DNA-wrapped SWCNT hybrids (DNA−SWCNTs).[4,5,8] A large molecular library is thus created as a result of the combinatorial diversity of nanotube structure and DNA sequence. Similar to globular-shaped peptide-based macromolecules, the tubular-shaped DNA−SWCNTs also possess surface morphologies that are dependent on the DNA folding on the SWCNT surfaces.[4,5,8,18,19] The basic premise of our sorting procedure is that an ordered DNA−SWCNT is formed only for a correct match between the DNA sequence and SWCNT structure and can be physically differentiated from all other DNA/SWCNT combinations. This approach, being combinatorial in nature, offers greater prospects than surfactant-based methods for fine structure resolution and recognition. In principle, any sequence-controlled polymer library could work in our approach. Nevertheless, nucleic acid polymers, being the first to emerge in the evolution of life from the inorganic world, may be uniquely suited for interfacing with inorganic surfaces. It is also rational to exploit the homochiral nature of DNA for SWCNT handedness control, since ultimately our ability to differentiate left- and right-handed structures originates from the homochiral nature of biomolecules.

This paper documents an extensive amount of work that we have conducted to illustrate the exquisite power of DNA in resolving both handedness and helicity of SWCNTs. We have screened over 300 DNA sequences using a recently developed aqueous two-phase (ATP) separation technique as an effective selection method. Additional experiments have also been carried out to reveal the physical mechanism of handedness resolution by DNA. Major findings are presented in the main text, but a substantial amount of experimental data are also included in the Supporting Information (SI).

Received: September 2, 2016
Published: December 12, 2016

DOI: 10.1021/jacs.6b09135
J. Am. Chem. Soc. 2016, 138, 16677−16685

MATERIALS AND METHODS

Stock DNA–SWCNT dispersions were prepared according to the previously published procedure.[20,21] Briefly, CoMoCAT SWCNT powders (SG65i grade, lot no. SG65i-L46, and EG150X grade, lot no. L4; Southwest Nanotechnologies) were dispersed in aqueous DNA (Integrated DNA Technologies) solutions containing 0.1 mol/L NaCl by sonication. Supernatants were collected after centrifugation for the selection experiments. The SWCNT/DNA mass ratio was 1:2 for all dispersions, with the SWCNT concentration being either 0.5 or 1 mg/mL. Various polymer ATP systems were used for SWCNT separation, including (1) a mixture of 7.76% poly(ethylene glycol) (PEG) (MW = 6 kDa, Alfa Aesar) and 15.0% polyacrylamide (PAM) (MW = 10 kDa, Sigma-Aldrich), denoted as PEG/PAM; (2) a mixture of 2.75% PEG, 2.75% poly(ethylene glycol) diamine (PEGDA) (MW = 6 kDa, Scientific Polymer Products, Inc.), and 7.50% dextran (DX) (MW ≈ 70 kDa, TCI), denoted as (PEG + PEGDA)/DX; and (3) a mixture of 5.50% PEG and 7.50% DX (PEG/DX). Both DX and poly(vinylpyrrolidone) (PVP) (MW = 10 kDa, Sigma-Aldrich) were used as DNA–SWCNT partition modulators. Sodium deoxycholate (SDC) (98%, BioXtra), sodium cholate hydrate (SC (>99%, BioXtra), and sodium dodecylbenzenesulfonate (SDBS) used for DNA/surfactant replacement were acquired from Sigma-Aldrich. All percentages specified for chemical concentration in aqueous solutions are reported on a mass basis.

UV–vis–NIR absorbance measurements were performed on a Varian Cary 5000 spectrophotometer over the wavelength range of 200–1400 nm using a 10 mm path length quartz microcuvette. Each purified (n,m) species was concentrated according to the SWCNT precipitation method reported previously[20−22] for the various UV–vis–NIR, circular dichroism (CD), near-infrared (NIR) fluorescence, and analytical ultracentrifugation (AUC) measurements. Unless indicated otherwise, after removal of the polymers through SWCNT precipitation, the resulting pellet containing the purified species was resuspended in water with the addition of the corresponding DNA sequence at a final concentration of 100 μg/mL to improve the dispersion stability.

CD spectra were recorded with an OLIS DSM 1000 CD spectrophotometer, covering a spectral range of 300 to 900 nm. All of the CD spectra were measured using 1.5 nm spectral steps and a circular quartz cell with an optical path length of 2 mm. With 0.6 mm spectral slits, the instrumental resolution was estimated to be approximately 2 nm.

NIR fluorescence spectra were acquired using a Horiba-Yvon Nanolog-3 spectrofluorometer equipped with a liquid-nitrogen-cooled 512-element InGaAs array detector. Excitation was selected with a 450 W xenon lamp and dual 1200 × 500 gratings. The resulting nanotube emission was collected at 90° and dispersed onto the detector array using a 150 × 1200 grating. The instrumental resolution was 6 nm for excitation and 8 nm for emission. The integration time ranged from 20 to 40 s depending on the concentration and quantum efficiency of the SWCNT samples. All of the emission spectra were corrected for detector train efficiency and lamp excitation.

RESULTS AND DISCUSSION

ATP as a Selection Scheme. A central task of our approach is to set up a selection process to identify ordered DNA–SWCNT structures among the many possible DNA/SWCNT combinations. This can be related to a general problem in molecular evolution: selection of macromolecules with defined structures from astronomical numbers of biopolymer sequences. We view DNA–SWCNTs as a model system for biomacromolecules: the regular geometry and structure-specific optical properties of the embedded SWCNTs[23] make it much easier to quantify population distributions during selection, to evaluate the overall structures of the selected species, and to analyze the mechanism of selection.

A number of selection processes for biopolymers have been explored.[24−26] A classic example is in vitro selection of aptamers from DNA or RNA sequence libraries,[25,26] in which a selected sequence binds to a target molecule on a stationary phase and is then separated from nonbinding sequences remaining in the corresponding mobile phase. This selection scheme has intrinsic limitations, since not all well-folded structures involve substrate binding. The ion-exchange chromatography (IEX) method we previously developed for SWCNT sorting[4,5,8] can also be viewed as a selection method, which has yielded the first successful purification of many semiconducting[8] and metallic species[27] with defined helicities. However, there are a number of disadvantages to the IEX-based method. First, the surface chemistry of the polymer beads that constitute the stationary phase is difficult to control, and as a result, inhomogeneous broadening of the interaction between the stationary phase and DNA–SWCNTs is often unavoidable. Second, the polymer beads change over time because of irreversible adsorption of DNA–SWCNTs. We realize that the binding-based and IEX-based selection schemes can be generalized by replacing the stationary and mobile phases with an ATP system[28] and by using preferential affinity to one of the two aqueous phases as the selection criterion (Scheme 1). ATP confers a number of advantages: (1) both phases are homogeneous, leading to elimination of inhomogeneous broadening in molecular interactions and thus improvement in resolution; (2) equilibrium partitioning depends on the solvation energy difference between two similar phases of microscale volumes, resulting in cancellation of many extrinsic factors (e.g., length) and higher reproducibility. These improvements are critical for achieving simultaneous resolution of handedness and helicity via ATP selection.

Scheme 1

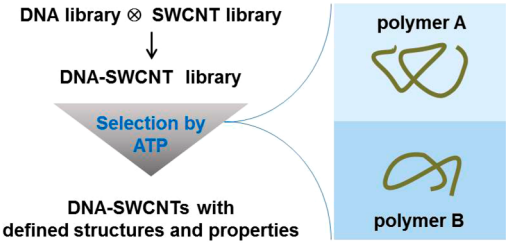

An ATP system exploits the polymer phase separation phenomenon to create two separate but permeable water phases of slightly different structures.[28] As a result, the hydration energy of a solute is rescaled differently in the two phases, leading to an uneven solute distribution. We recently conducted a study of DNA–SWCNT partitioning in various ATP systems[20] and demonstrated a strong dependence of the DNA–SWCNT partitioning on the DNA sequence and SWCNT structure. We additionally showed that the polymer composition can be used to rescale the hydration energies and modulate the DNA–SWCNT partitioning. For example, addition of DX to a PEG/PAM system makes the bottom phase more hydrophilic and pulls down DNA–SWCNTs from the top to the bottom phase; addition of PVP conversely brings nanotubes from the bottom to the top phase. These measures are similar to stringency adjustment in binding-based selections. With a proper choice of polymers such as PEGDA, one may also incorporate electrostatic binding into partition control

DOI: 10.1021/jacs.6b09135
J. Am. Chem. Soc. 2016, 138, 16677–16685

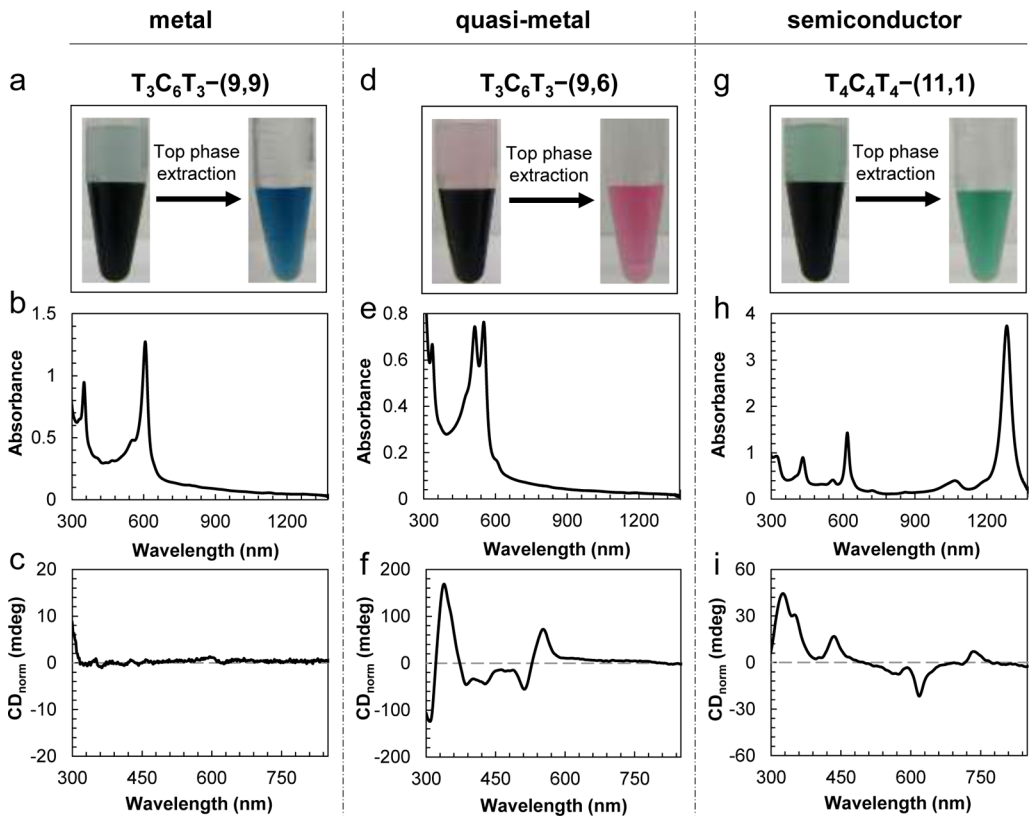

Figure 1. Examples of DNA–SWCNT selection by ATP systems. (a) Left photograph: partition of $T_3C_6T_3$ SWCNTs (final concentration ≈ 0.15 mg/mL) in a poly(ethylene glycol) (PEG)/polyacrylamide (PAM) system, with (9,9) species found in the PEG-rich top phase. Right photograph: extracted and concentrated (9,9) species. (b) Absorbance spectrum of the concentrated (9,9) species. (c) CD spectrum of the (9,9) species. (d) Left photograph: partition of $T_3C_6T_3$ SWCNTs (final concentration ≈ 0.15 mg/mL) in a PEG/dextran (DX) system with a final polyvinylpyrrolidone (PVP) concentration of 0.12%, with (9,6) species found in the PEG-rich top phase. Right photograph: extracted and concentrated (9,6) species. (e) Absorbance spectrum of the concentrated (9,6) species. (f) CD spectrum of the (9,6) species. (g) Left photograph: partition of $T_4C_4T_4$ SWCNTs (final concentration ≈ 0.15 mg/mL) in a PEG/PAM system, with (11,1) species found in the PEG-rich top phase. Right photograph: extracted and concentrated (11,1) species. (h) Absorbance spectrum of the concentrated (11,1) species. (i) CD spectrum of the (11,1) species. Additional experimental details are included in the SI.

mechanisms. These options give ATP selection a broader operational range than traditional binding-based selection.[24−26]

A Systematic but Limited Search of the DNA Sequence Space. To explore the potential of ATP selection in handling the vast DNA–SWCNT library, we conducted a systematic but limited search of the DNA sequence space. To restrict the scope of the search, we focused mainly on short sequences that conform to a palindromic pattern (see the SI for details). This is an effective way to cover the sequence space, since in a given library of N random DNA sequences there exist only $\sim N^{1/2}$ that are palindromic. To further limit the scope of our search, we examined only single-nucleotide repeats and sequences composed of two types of nucleotides, i.e., T/A, G/T, G/C, G/A, A/C, and T/C sublibraries.

A total of over 300 sequences were examined. We used each test sequence to disperse a synthetic SWCNT mixture and then loaded the dispersion into an ATP system. We used absorption spectroscopy to monitor the SWCNT helicity distribution[23] in the ATP system and adjusted the polymer composition to minimize the number of species in one of the phases. The explicit selection criterion targets SWCNTs with a defined chiral index (n, m). For most of the tested sequences (~90%), a mixture of SWCNTs is always found in both phases. For some special sequences (~10%), only one major SWCNT species is found in either the top or bottom phase. Figure 1 illustrates three examples of these special sequences that allow selection of SWCNTs from three distinct electronic types: metal, quasi-metal, and semiconductor. In all three cases, the selected species are partitioned into the top phase of either a PEG/PAM or PEG/DX system and separated from the rest of the population in the bottom phase. While these examples demonstrate the extraction of the most hydrophobic species, we also found cases where a single most hydrophilic species can be extracted from the bottom phase.

The explicit criterion of our selection ensures that only one SWCNT species with fixed chiral index (n, m) is selected. However, this criterion does not uniquely define the SWCNT structure, since both left- and right-handed configurations are possible. We found by CD measurements that all of the selected DNA–SWCNTs are highly enriched in either left- or right-handed forms for chiral tubes (Figure 1f,i). This is in contrast to some IEX-selected DNA–SWCNTs, which do not have clearly defined handedness.[29] To confirm that the observed CD signal was not induced by the chiral DNA, we conducted additional CD measurements after displacing the DNA with the achiral surfactant SDBS (Figure S28). Negligible differences in intensity were observed after surfactant exchange, indicating that the CD was indeed intrinsic to the nanotubes.

Wide Selection Range in the SWCNT Chirality Space. A selection procedure may be intrinsically biased toward a

DOI: 10.1021/jacs.6b09135
J. Am. Chem. Soc. 2016, 138, 16677−16685

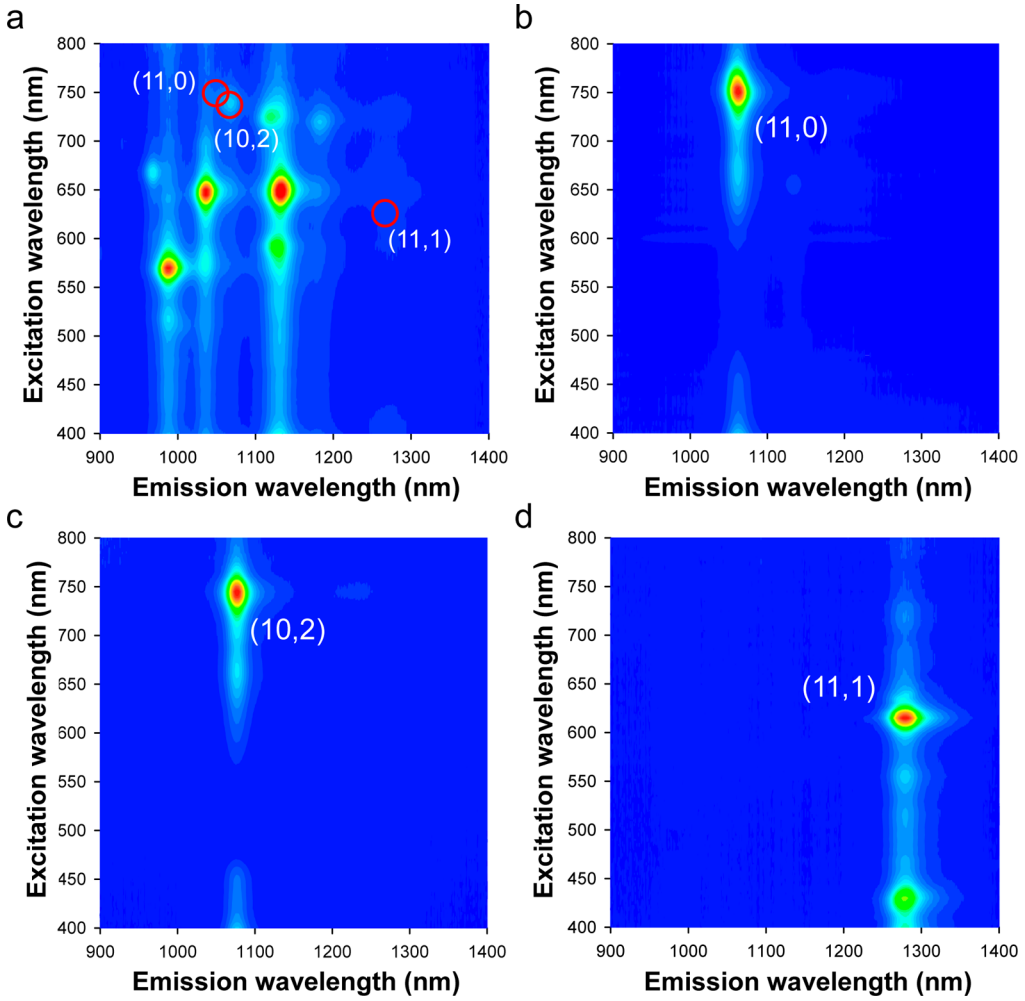

Figure 2. Photoluminescence 2D excitation−emission maps of the parent synthetic mixture and ATP-selected single-chirality species. (a) Parent synthetic mixture containing many SWCNT species. (b−d) Low-abundance species (11,0) (b), (10,2) (c), and (11,1) (d) selectively extracted from the parent shown in (a) using PEG/PAM systems (see the SI for details). The photoluminescence is normalized by the peak emission intensity in each plot. Red circles in (a) denote the spectral positions of the extracted single-chirality species in (b−d). The emission intensity qualitatively reflects the relative abundance of each species.

certain range of the candidate pool. We found that ATP selection does not have any structural bias as far as SWCNT helicity is concerned. Figure 2a shows a two-dimensional (2D) excitation−emission photoluminescence map (PL-map) of a typical SWCNT synthetic mixture containing many species of different helicities, with near-armchair tubes being more abundant than zigzag tubes. The PL-maps in Figure 2b−d illustrate that even low-abundance species such as (10,2), (11,0), and (11,1) (isolated from the parent mixture in Figure 2a) can be efficiently selected with the correctly chosen DNA sequence. Figure 3 shows the CD spectra and corresponding absorption spectra of 23 distinct SWCNT species that we have isolated to date, including armchair metals, non-armchair quasi-metals, and semiconducting tubes with chiral angles ranging from pure zigzag to near-armchair. A detailed description of the polymer systems and separation procedures applied for the isolation of each SWCNT species can be found in the SI. In order to compare the relative enantiomeric purities, the CD spectra were normalized (CD_{norm}) by the absorption of the E_{22} electronic transition (M_{11} for metallic species). Table 1 lists the recognition sequences used for ATP selection and summarizes the CD_{norm} values obtained from the isolated species in this work. We found that the normalized CD intensities of many of the selected nanotube enantiomers surpass the highest values available from the literature.[12−14] (Higher enantiomer purities for semiconducting SWCNTs were reported by Wei et al.[30] after the submission of this article and are included in Table 1). These results are remarkable since none of the previously reported SWCNT sorting methods provides such a broad range of coverage in chirality space.[8,9,13]

Quasi-Metal Species. The four purified quasi-metal species (7,4), (8,5), (9,6), and (11,2) shown in Figure 4 deserve special attention. SWCNTs are often classified as either metals or semiconductors. However, evidence is emerging that true metals of armchair type can be chemically differentiated from quasi-metals of non-armchair type.[31,32] Functionally, quasi-metals are essentially narrow-band-gap semiconducting species that are potentially useful materials for far-infrared and terahertz devices. Spectroscopically, quasi-metals have distinct features that differ from armchair metals. Trigonal warping effects are predicted not only to open up a band gap in quasi-metal SWCNTs but also to split the M_{11} optical transition (ΔE_{11}^{M}) by an amount that scales with $\cos(3\alpha)/d^2$, where α is the chiral angle and d is the tube diameter.[33−35] We obtain ΔE_{11}^{M} values for each quasi-metal species by measuring the difference in energy between the M_{11}^{+} and M_{11}^{-} peaks (Table 2).

DOI: 10.1021/jacs.6b09135
J. Am. Chem. Soc. 2016, 138, 16677−16685

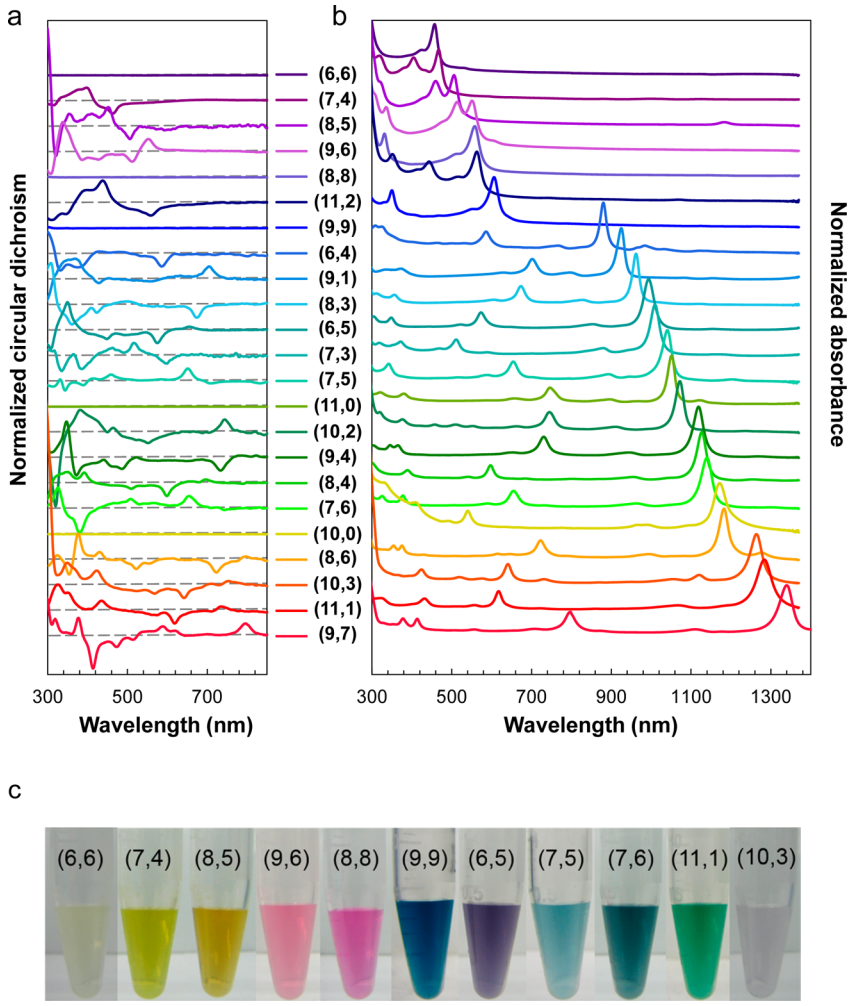

Figure 3. Optical characterization of distinct SWCNT species selected by ATP. (a) CD spectra of the selected SWCNT species. Only one of the enantiomers is included for (9,6), (8,3), (6,5), and (7,6). CD spectra from chiral species are normalized at the E_{22} peak position (M_{11} for metallic species). For achiral species, the original CD spectra are plotted. Dashed gray lines correspond to the zero baselines. We note that the CD spectra reveal many electronic transitions not observable in other optical measurements, and analysis of these transitions may yield new information about the electronic structures of SWCNTs. (b) Corresponding absorbance spectra of the selected SWCNT species. Each spectrum is normalized at the E_{11} peak position, and the spectra have been offset for easy comparison. Original CD and absorbance spectra for each species are included in the SI. (c) Photographs of a subset of purified SWCNT species.

These values are plotted versus $\cos(3\alpha)/d^2$ in the inset of Figure 4 and show a clear linear trend, confirming the aforementioned theoretical prediction. We also found that our measured ΔE_{11}^{M} values correlate well with those calculated from the empirical formula reported by Liu et al.[34] We anticipate that our selection procedure will enable isolation of additional quasi-metallic species and facilitate further study of this unique electronic type of SWCNTs.

SWCNT Handedness Recognition by DNA. To reveal the mechanism of handedness selection, we conducted a detailed study of enantiomer recognition by the palindromic sequence TTA TAT TAT ATT. A (−) (6,5) hybrid and its mirror image (+) (6,5) (see the Table 1 footnote for the sign convention) were obtained via a multistage selection process as the most hydrophobic and most hydrophilic species, respectively, among all of the TTA TAT TAT ATT–SWCNT hybrids in a PEG/PAM system (see the SI for details). CD measurements (Figure 5a) confirmed the opposite handedness of the two enantiomers, and the signal intensities normalized by the E_{22} absorbance showed near record-high values. Quantitative analysis also indicated that the enantiomeric excess for both species is >90% (see the SI).

We characterized the (6,5) enantiomer hybrids using NIR photoluminescence (PL) spectroscopy. Because of the sensitivity of nanotube PL, small perturbations in the external environment are readily observed in the form of spectral variations. PL-maps (Figure 5b,c; also see the SI) show that the E_{11} emission peak of the (−) (6,5) enantiomer has a narrower line width, is blue-shifted by 5 nm, and is 1.7 times stronger in intensity compared with that of the (+) (6,5) enantiomer. These data suggest that the dielectric environments shaped by the folding structure of the same DNA sequence are drastically different for the two enantiomers. We have compared these spectral changes to additional PL measurements acquired for the same (6,5) enantiomers after the DNA was exchanged with both chiral SC and SDC and achiral SDBS surfactants (see the SI). Figures 6 and S29 show that spectral differences in shape, intensity, and peak position are also observed when the (6,5) enantiomers are coated by chiral SC and SDC. Similar to DNA, we attribute these variations to differences in packing structure, as each chiral dispersant is able to differentiate structural

DOI: 10.1021/jacs.6b09135
J. Am. Chem. Soc. 2016, 138, 16677−16685

Table 1. List of DNA Recognition Sequences for the ATP-Selected SWCNT Species and the Corresponding Normalized CD Intensities in Comparison with Literature Values

SWCNT[a]	DNA sequence	E_{22} (M_{11}) CD_{norm} (mdeg)	highest reported E_{22} CD_{norm} (mdeg)	yield (%)[b]
achiral (6,6)	$CTTC_3TTC$	0	–	1.6
(−) (7,4)	$CTTC_3TTC$, $(TCG)_4TC$	−86	–	4.5
(−) (8,5)	$TC_{10}T$, $T_3C_6T_3$	−7	–	6.9
(±) (9,6)	$T_3C_6T_3$, $(TG)_2T_4(GT)_2$	+72, −26	–	1.5
achiral (8,8)	C_5TTC_5	0	–	1.8
(−) (11,2)	$CTTC_6TTC$	−45	–	0.3
achiral (9,9)	$T_3C_6T_3$	0	–	2.4
(−) (6,4)	$A_3T_6A_3$	−33	+62, −61[d]	2.7
(+) (9,1)	$(GTC)_2GT$, $(TG)_2T_4(GT)_2$	+16	+13, −21[d]	1.6
(±) (8,3)	$CTTC_2TTC$, $(TCG)_4TC$, $(TTA)_2(ATT)_2$	+41, −32	+41, −50[d]	4.4
(±) (6,5)	$TTA(TAT)_2ATT$ and 10 other sequences (see the SI)	±84	+93, −85[d]	(−) 6,5: 19.3 (+) 6,5: 12.4
(+) (7,3)	$TCT(CTC)_2TCT$	+9	+55, −56[d]	8.7
(+) (7,5)	$(ATT)_4$, $TGG(GTG)_2GGT$	+78	+27, −61[d]	6.0
achiral (11,0)	GC_{11}, C_{12}, TC_6T, $AC_{10}A$, AC_{11}	0	–	0.9
(+) (10,2)	$(TC)_3CTCCCT$	+19	+22, −27[d]	1.9
(−) (9,4)	$CTTC_3TTC$, TTC_4TT	−32	+81, −4[c]	4.3
(−) (8,4)	$(GT)_{20}$, TC_5T	−82	+87, −81[d]	2.7
(±) (7,6)	CTC_3TC, $T_3C_5T_3$	+25, −19	+73, −42[d]	11.7
achiral (10,0)	$(TTA)_3TTGTT$	0	–	0.7
(−) (8,6)	$(TCT)_2$	−45	−4[c]	1.2
(−) (10,3)	C_5TC_6	−37	+61[d]	1.6
(−) (11,1)	$T_4C_4T_4$	−22	+12, −19[d]	1.2
(+) (9,7)	C_5TTC_5	+45	–	1.1

[a]The plus or minus sign of each SWCNT species is assigned according to the sign of the CD value at the E_{22} (M_{11} for metallic species) position. [b]The estimation of the % yield is given for the first DNA sequence listed and is calculated for the (n, m) species over the total CNT mass in the starting material. A detailed description of the method is given in ref 20. [c]From ref 14. [d]From ref 30.

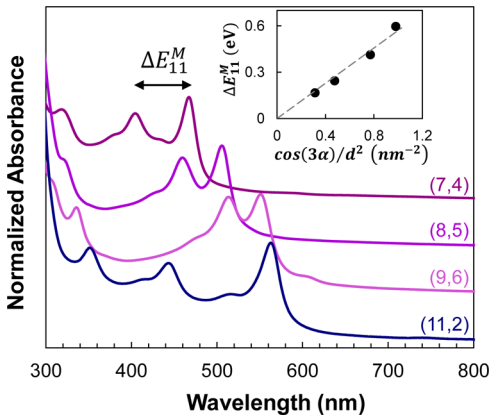

Figure 4. Spectral splitting of the first exciton transitions in quasi-metals. Normalized absorbance spectra of $CTTC_3TTC$-(7,4), $TC_{10}T$-(8,5), $T_3C_6T_3$-(9,6), and $CTTC_6TTC$-(11,2). The inset shows a plot of the measured ΔE_{11}^M vs $\cos(3\alpha)/d^2$, where α is the nanotube chiral angle and d is the nanotube diameter. The best linear fit shown by the dashed line yields a slope of 0.57 and R^2 = 0.9738.

Table 2. Measured M_{11} and ΔE_{11}^M Values and Corresponding Calculated ΔE_{11}^M Values[34]

SWCNT	λ_{11}^{M-} (nm)	λ_{11}^{M+} (nm)	ΔE_{11}^M (eV)	calcd ΔE_{11}^M (eV)
(7,4)	467	404	0.414	0.419
(8,5)	506	460	0.245	0.259
(9,6)	551	513	0.167	0.171
(11,2)	563	443	0.597	0.534

handedness. Indeed, SC and SDC are both commonly applied surfactants that have been successively demonstrated to separate SWCNTs by helicity and handedness.[12−14] On the other hand, the emission spectra of the (6,5) enantiomers are nearly identical when they are coated by the achiral surfactant SDBS, as expected, indicating that the spectral differences are not due to a difference in SWCNT quality but are the result of the same differentiation in surface coating that leads to the ATP separation. We note that the spectral differences are the most pronounced when the SWCNTs are wrapped in DNA, suggesting that DNA may be superior to small-molecule surfactants in enantiomer differentiation.

Much more dramatic differences are observed in comparisons of chemical reactivity. Figure 5d shows the results of an oxidation reaction[36] between NaClO and the two DNA−enantiomer hybrids. By quantifying the degree of oxidation according to the E_{11} absorption peak intensity change, we observe that the (+) (6,5) enantiomer is much more susceptible to oxidation than the (−) (6,5) one: at 0.5 mM NaClO, the former is 80% oxidized (Figure 5e), whereas the latter is only 10% oxidized (Figure 5f). We attribute these differences in chemical reactivity to variations in nanotube surface exposure, i.e., better coverage of the DNA on the (−) (6,5) hybrid prevents electron transfer reactions from occurring compared with the (+) (6,5) hybrid, whose surface is more exposed and thus accessible to NaClO. Greater exposure to the high dielectric environment of water should lead to a lower PL intensity and red-shifted emission,[37] which was indeed observed in our PL measurements as mentioned above.

We carried out further characterization by AUC measurements to determine the anhydrous densities (density of the

DOI: 10.1021/jacs.6b09135
J. Am. Chem. Soc. 2016, 138, 16677−16685

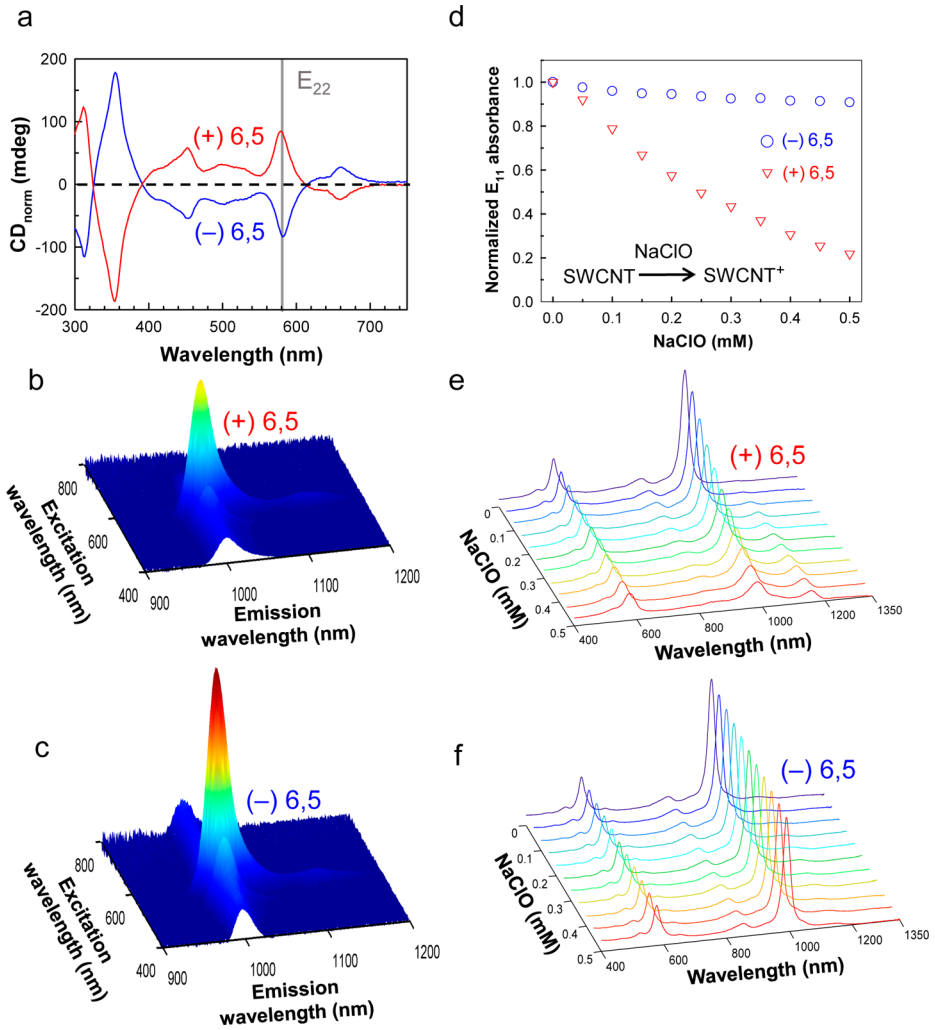

Figure 5. Optical characterization and differential chemical reactivity of DNA–SWCNT enantiomer hybrids. (a) CD measurement of TTA TAT TAT ATT-(6,5) enantiomer hybrids selectively isolated from a multistage extraction process in a PEG/PAM system. The (+) (6,5) and (−) (6,5) enantiomers (referenced by the sign of their E_{22} CD peaks; solid gray vertical line) show nearly equal intensities but opposite signs. For better comparison, the CD intensity has been normalized by the E_{22} absorption. To confirm that the CD signal is intrinsic to the nanotubes and not induced by the chiral DNA, additional CD measurements on the (−) (6,5) enantiomer were acquired after the DNA was displaced with an achiral surfactant (see the SI). (b, c) Photoluminescence 3D excitation–emission maps of the (+) (6,5) (b) and (−) (6,5) (c) enantiomers. We observe that the E_{11} fluorescence emission peak of the (−) (6,5) enantiomer is 1.7 times brighter, blue-shifted by 5 nm, and 6 nm more narrow (full width at half-maximum) relative to the (+) (6,5) enantiomer. (d–f) Oxidation reaction between NaClO and the (+) (6,5) (e) and (−) (6,5) (f) enantiomers. The extent of oxidation was monitored by the bleaching of the E_{11} absorption peak (d). At 0.5 mM NaClO the (+) (6,5) is 80% oxidized while the (−) (6,5) is only 10% oxidized.

DNA–SWCNT complex without any contributions from the associated hydration shell) of the (+) (6,5) and (−) (6,5) enantiomer hybrids. Sedimentation coefficients (s) were measured for each sample in solutions of varying H_2O to D_2O ratio. To find the anhydrous density, the solution-viscosity-corrected sedimentation coefficient s was plotted against solution density (Figure S32) and extrapolated to the y-intercept, at which $s = 0$. Additional details pertaining to the AUC measurements can be found in the SI. We found that the anhydrous densities of the two enantiomer hybrids are significantly different, with the (−) (6,5) hybrid (1988 kg/m^3) possessing a higher anhydrous density than the (+) (6,5) hybrid (1845 kg/m^3). Given that the densities of the bare (6,5) enantiomers are the same, the differences in anhydrous density must arise from variations in DNA structure on the two (6,5) enantiomer hybrids.

Taken together, our results suggest that in the (6,5) enantiomer complexes, the DNA conformation bears an epitaxial relationship with the embedded SWCNT, thus resulting in different folding structures on each enantiomer hybrid. Enantiomer differentiation by DNA renders different physical and chemical properties to left- and right-handed DNA–SWCNT hybrids. Our findings establish a first example of functionally distinguishable left- and right-handed SWCNTs and highlight the need to control SWCNT handedness in studying the interactions of nanotubes with other molecules, particularly homochiral biomacromolecules.

A Hydration-Energy-Driven Selection Mechanism. How does the difference in DNA wrapping structure on different enantiomers translate into a partition difference in the ATP selection? Why is the ATP selection effective in isolating nanotubes of defined helicity and handedness? These questions prompted us to develop a quantitative analysis to understand

DOI: 10.1021/jacs.6b09135
J. Am. Chem. Soc. 2016, 138, 16677–16685

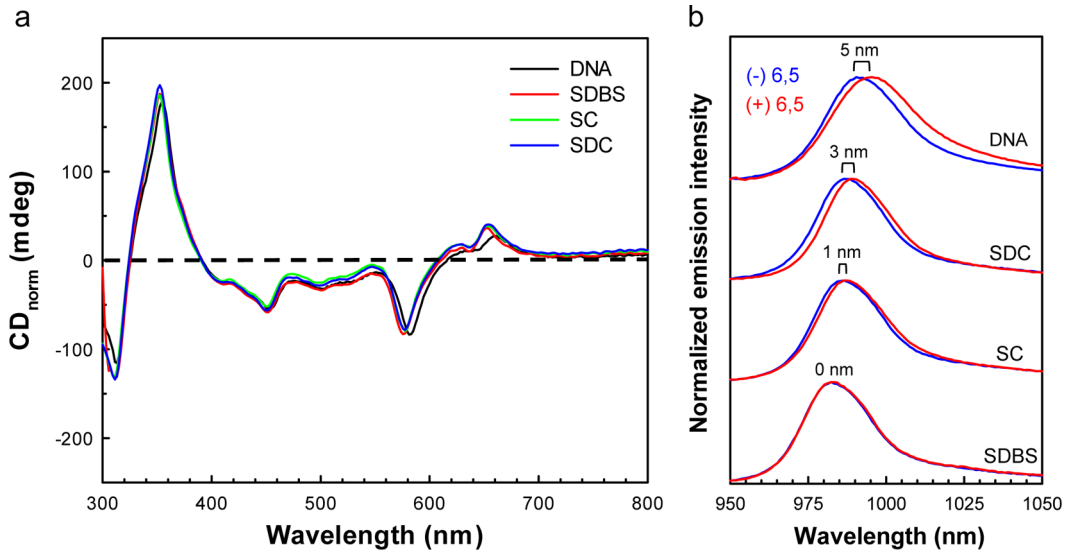

Figure 6. Optical characterization of (6,5) SWCNT enantiomers coated with DNA and various surfactants. (a) CD measurements of the (−) (6,5) TTA TAT TAT ATT enantiomer after the DNA was displaced with different chiral (SC and SDC) and achiral (SDBS) surfactants. Negligible changes in CD intensity are observed, confirming that the CD is intrinsic to the nanotube sample.(b) Comparison of fluorescence spectra for the (−) (6,5) and (+) (6,5) enantiomers coated with TTA TAT TAT ATT and with different surfactants after DNA replacement. The largest variations in peak position and spectral width are observed when the enantiomers are wrapped in DNA. All of the spectra have been normalized by the peak emission intensity. The peak position differences between the two enantiomers are 5, 3, 1, and 0 nm for DNA, SDC, SC, and SDBS, respectively.

the underlying mechanism, the details of which will be published elsewhere. Here we present some basic notions of the analysis. We first note that even though partitioning of an analyte in an ATP system is determined by the difference between the analyte's solvation energies in the two phases, empirical observations suggest[28,38] that the partitioning is correlated with the hydration energy or hydrophilicity/hydrophobicity level of the analyte. In our experimental setup, a DNA−SWCNT is selected when it is partitioned into either the top or bottom phase exclusively and is well-separated from other species. This implies that hydration energy of the selected species must not only have an extreme value[28,38] but also be well-separated from those of other DNA−SWCNT hybrids in the dispersed population. In view of the sensitivity of the hydration energy to minute structure variations,[10,20] this requires the selected species to have minimum structural variation, or minimum conformational entropy, to avoid overlapping partitioning with other species. Thus, minimum conformational entropy is an implicit selection criterion. Two sources of structure variation contribute to the conformational entropy of a DNA−SWCNT. First, a SWCNT may have either a left- or right-handed configuration. Second, DNA folding may have a distribution of conformations populated at room temperature. Reducing ambiguity in SWCNT handedness is one way to minimize conformational entropy; another is to have a DNA sequence that adopts a well-defined folding conformation and chiral character commensurate with the encased SWCNT. We suggest that both need to happen in order to ensure selection of SWCNTs with defined handedness. Our case is analogous to the folding of biopolymers, where substrate stereoselectivity is a natural outcome of a well-folded structure built by homochiral monomers.

CONCLUSION AND OUTLOOK

The results presented in this paper demonstrate that specific sequences of homochiral DNA are very effective in recognizing both handedness and helicity of SWCNTs. Even though simultaneous handedness and helicity enrichment of semiconducting SWCNTs have been achieved by small-molecule surfactants, our findings nevertheless constitute a first comprehensive method for simultaneous handedness and helicity enrichment for all three electronic types of SWCNTs. Thus, this work represents an important milestone reached in the quest for solving the structural polydispersity problem of SWCNTs.

Our findings are enabled by the ATP separation method. During the course of this work, we have come to the conceptual realization that ATP separation is an effective method for the selection of macromolecules with defined structures and properties. The exquisite selectivity of ATP selection is attributed to the sensitive dependence of hydration interactions on minute structure variations, which is enacted in some unknown way by the peculiar quantum-chemical behavior of liquid water. Further studies are needed to delineate the potential and limitations of water in structure resolution. On the practical side, ATP selection may be extended to the identification of structures that bind to specific target molecules tagged on one of the two polymers in an ATP system. Well-developed PEGylation techniques may prove especially useful in this regard. Finally, the availability of handedness- and helicity-controlled SWCNT materials of all three electronic types should open up new possibilities in SWCNT stereochemistry, biosensing, and electronic[39,40] and optoelectronic[41,42] applications.

ASSOCIATED CONTENT

Supporting Information

The Supporting Information is available free of charge on the ACS Publications website at DOI: 10.1021/jacs.6b09135.

Materials and Methods, Figures S1−S32, and Tables S1−S4 (PDF)

DOI: 10.1021/jacs.6b09135
J. Am. Chem. Soc. 2016, 138, 16677−16685

AUTHOR INFORMATION

Corresponding Author

*ming.zheng@nist.gov

ORCID

Jeffrey A. Fagan: 0000-0003-1483-5554

Ming Zheng: 0000-0002-8058-1348

Author Contributions

†G.A. and J.K.S. contributed equally.

Notes

The authors declare no competing financial interest.

ACKNOWLEDGMENTS

We thank Drs. Anand Jagota and Jack Douglas for their critical reading of the manuscript. This work was supported in part by a grant from AFOSR. J.K.S. acknowledges a National Research Council postdoctoral fellowship.

REFERENCES

(1) Liu, J.; Wang, C.; Tu, X.; Liu, B.; Chen, L.; Zheng, M.; Zhou, C. *Nat. Commun.* **2012**, *3*, 1199.

(2) Yang, F.; Wang, X.; Zhang, D.; Yang, J.; Luo, Da; Xu, Z.; Wei, J.; Wang, J.-Q.; Xu, Z.; Peng, F.; Li, X.; Li, R.; Li, Y.; Li, M.; Bai, X.; Ding, F.; Li, Y. *Nature* **2014**, *510*, 522.

(3) Sanchez-Valencia, J. R.; Dienel, T.; Groning, O.; Shorubalko, I.; Mueller, A.; Jansen, M.; Amsharov, K.; Ruffieux, P.; Fasel, R. *Nature* **2014**, *512*, 61.

(4) Zheng, M.; Jagota, A.; Semke, E. D.; Diner, B. A.; McLean, R. S.; Lustig, S. R.; Richardson, R. E.; Tassi, N. G. *Nat. Mater.* **2003**, *2*, 338.

(5) Zheng, M.; Jagota, A.; Strano, M. S.; Santos, A. P.; Barone, P.; Chou, S. G.; Diner, B. A.; Dresselhaus, M. S.; McLean, R. S.; Onoa, G. B.; Samsonidze, G. G.; Semke, E. D.; Usrey, M.; Walls, D. J. *Science* **2003**, *302*, 1545.

(6) Arnold, M. S.; Green, A. A.; Hulvat, J. F.; Stupp, S. I.; Hersam, M. C. *Nat. Nanotechnol.* **2006**, *1*, 60.

(7) Nish, A.; Hwang, J.-Y.; Doig, J.; Nicholas, R. J. *Nat. Nanotechnol.* **2007**, *2*, 640.

(8) Tu, X.; Manohar, S.; Jagota, A.; Zheng, M. *Nature* **2009**, *460*, 250.

(9) Liu, H.; Nishide, D.; Tanaka, T.; Kataura, H. *Nat. Commun.* **2011**, *2*, 309.

(10) Khripin, C. Y.; Fagan, J. A.; Zheng, M. *J. Am. Chem. Soc.* **2013**, *135*, 6822.

(11) Peng, X.; Komatsu, N.; Bhattacharya, S.; Shimawaki, T.; Aonuma, S.; Kimura, T.; Osuka, A. *Nat. Nanotechnol.* **2007**, *2*, 361.

(12) Green, A.; Duch, M.; Hersam, M. *Nano Res.* **2009**, *2*, 69.

(13) Ghosh, S.; Bachilo, S. M.; Weisman, R. B. *Nat. Nanotechnol.* **2010**, *5*, 443.

(14) Liu, H.; Tanaka, T.; Kataura, H. *Nano Lett.* **2014**, *14*, 6237.

(15) Akazaki, K.; Toshimitsu, F.; Ozawa, H.; Fujigaya, T.; Nakashima, N. *J. Am. Chem. Soc.* **2012**, *134*, 12700.

(16) Tanaka, T.; Urabe, Y.; Hirakawa, T.; Kataura, H. *Anal. Chem.* **2015**, *87*, 9467.

(17) Magg, M.; Kadria-Vili, Y.; Oulevey, P.; Weisman, R. B.; Bürgi, T. *J. Phys. Chem. Lett.* **2016**, *7*, 221.

(18) Roxbury, D.; Tu, X.; Zheng, M.; Jagota, A. *Langmuir* **2011**, *27*, 8282.

(19) Shankar, A.; Mittal, J.; Jagota, A. *Langmuir* **2014**, *30*, 3176.

(20) Ao, G.; Khripin, C. Y.; Zheng, M. *J. Am. Chem. Soc.* **2014**, *136*, 10383.

(21) Ao, G.; Zheng, M. *Curr. Protoc. Chem. Biol.* **2015**, *7*, 43.

(22) Khripin, C. Y.; Arnold-Medabalimi, N.; Zheng, M. *ACS Nano* **2011**, *5*, 8258.

(23) Bachilo, S. M.; Strano, M. S.; Kittrell, C.; Hauge, R. H.; Smalley, R. E.; Weisman, R. B. *Science* **2002**, *298*, 2361.

(24) Smith, G. P. *Science* **1985**, *228*, 1315.

(25) Ellington, A. D.; Szostak, J. W. *Nature* **1990**, *346*, 818.

(26) Tuerk, C.; Gold, L. *Science* **1990**, *249*, 505.

(27) Tu, X.; Hight Walker, A. R.; Khripin, C. Y.; Zheng, M. *J. Am. Chem. Soc.* **2011**, *133*, 12998.

(28) Albertsson, P.-A. *Partition of Cell Particles and Macromolecules*, 2nd ed.; Wiley-Interscience: New York, 1971.

(29) Dukovic, G.; Balaz, M.; Doak, P.; Berova, N. D.; Zheng, M.; Mclean, R. S.; Brus, L. E. *J. Am. Chem. Soc.* **2006**, *128*, 9004.

(30) Wei, X.; Tanaka, T.; Yomogida, Y.; Sato, N.; Saito, R.; Kataura, H. *Nat. Commun.* **2016**, *7*, 12899.

(31) Hároz, E. H.; Rice, W. D.; Lu, B. Y.; Ghosh, S.; Hauge, R. H.; Weisman, R. B.; Doorn, S. K.; Kono, J. *ACS Nano* **2010**, *4*, 1955.

(32) Gui, H.; Streit, J. K.; Fagan, J. A.; Hight Walker, A. R.; Zhou, C.; Zheng, M. *Nano Lett.* **2015**, *15*, 1642.

(33) Kane, C. L.; Mele, E. J. *Phys. Rev. Lett.* **1997**, *78*, 1932.

(34) Liu, K.; Deslippe, J.; Xiao, F.; Capaz, R. B.; Hong, X.; Aloni, S.; Zettl, A.; Wang, W.; Bai, X.; Louie, S. G.; Wang, E.; Wang, F. *Nat. Nanotechnol.* **2012**, *7*, 325.

(35) Haroz, E. H.; Duque, J. G.; Tu, X.; Zheng, M.; Hight Walker, A. R.; Hauge, R. H.; Doorn, S. K.; Kono, J. *Nanoscale* **2013**, *5*, 1411.

(36) Zheng, M.; Diner, B. A. *J. Am. Chem. Soc.* **2004**, *126*, 15490.

(37) Bergler, F. F.; Schöppler, F.; Brunecker, F. K.; Hailman, M.; Hertel, T. *J. Phys. Chem. C* **2013**, *117*, 13318.

(38) Zaslavsky, B. Y. *Aqueous Two-Phase Partitioning*; Marcel Dekker: New York, 1994.

(39) Diniz, G. S.; Latgé, A.; Ulloa, S. E. *Phys. Rev. Lett.* **2012**, *108*, 126601.

(40) Alam, K. M.; Pramanik, S. *Adv. Funct. Mater.* **2015**, *25*, 3210.

(41) Ma, X.; Hartmann, N. F.; Baldwin, J. K. S.; Doorn, S. K.; Htoon, H. *Nat. Nanotechnol.* **2015**, *10*, 671.

(42) Shi, Z.; Hong, X.; Bechtel, H. A.; Zeng, B.; Martin, M. C.; Watanabe, K.; Taniguchi, T.; Shen, Y.-R.; Wang, F. *Nat. Photonics* **2015**, *9*, 515.

DOI: 10.1021/jacs.6b09135
J. Am. Chem. Soc. 2016, 138, 16677−16685